ELSEVIER

Earth and Planetary Science Letters 196 (2002) 99–111

EPSL

www.elsevier.com/locate/epsl

Factors contributing to high $\delta^{13}C$ values in Cryogenian limestones of western Mongolia

Graham A. Shields [a,*], Martin D. Brasier [b], Peter Stille [c], Dorj-iin Dorjnamjaa [d]

[a] *Ottawa-Carleton Geoscience Centre, University of Ottawa, P.O. Box 450, Stn. A, Ottawa, ON, Canada K1N 6N5*
[b] *Department of Earth Sciences, University of Oxford, Parks Road, Oxford OX1 3PR, UK*
[c] *Centre de Géochimie de la Surface (E.O.S.T./UMR 7517), 1 rue Blessig, 67084 Strasbourg, France*
[d] *Institute of Geology, Academy of Sciences, P.O. Box 863, Ulaanbaatar 210613, Mongolia*

Received 13 April 2001; received in revised form 10 October 2001; accepted 19 December 2001

Abstract

A geochemical study of Cryogenian (late Neoproterozoic) limestones from western Mongolia is presented, including $\delta^{13}C$ (carbonate and kerogen), $\delta^{18}O$, $^{87}Sr/^{86}Sr$ and rare earth element data. Carbon isotope compositions confirm the existence of anomalously high $\delta^{13}C$ in Cryogenian seawater with $\delta^{13}C_{carb} > +10‰$. Positive $\delta^{13}C$ excursions are explained conventionally by elevated rates of organic carbon burial. However, four additional factors appear likely to have contributed to $\delta^{13}C$ excursions during the Cryogenian: (1) increased $\delta^{13}C$ of carbon input (δ_i) due to the exposure and weathering of carbonate platforms during sea-level falls, (2) increased carbon isotopic discrimination between carbonates and organic carbon ($\Delta\delta^{13}C$) due to microbial reworking of primary organic matter, (3) locally elevated $\delta^{13}C$ in restricted basins and (4) enhanced vertical gradients in seawater $\delta^{13}C$ due to redox stratification. All four factors may have contributed to similar positive $\delta^{13}C$ excursions at other times, and may help to explain the almost ubiquitous association of eustatic regression, and cooling, with high $\delta^{13}C$ during the late Neoproterozoic and early Palaeozoic.

Keywords: carbon; stable isotopes; cerium; anomalies; Neoproterozoic; Mongolia; limestone

1. Introduction

The late Neoproterozoic (750–543 Ma) is being increasingly recognized as a key interval in Earth history, during which there was widespread continental break-up and dispersal [1], repeated glaciation [2–4] and the beginnings of metazoan evolution [5]. Carbon isotope variations in seawater have become important tools to understand Neoproterozoic environmental change because of the anomalously high (and low) $\delta^{13}C$ values that have been reported from Neoproterozoic carbonate rocks [3,4,6]. Marine carbonate $\delta^{13}C$ is interpreted conventionally with the help of the following mass

* Corresponding author. Present adress: Department of Earth Sciences, James Cook University, Townsville, Queensland 4811, Australia.
E-mail addresses: graham.shields@jcu.edu.au (G.A. Shields), martin.brasier@earth.ox.ac.uk (M.D. Brasier), pstille@illite.u-strasbg.fr (P. Stille), icbm@magicnet.mn (D.-i. Dorjnamjaa).

0012-821X/02/$ – see front matter
PII: S0012-821X(02)00461-2

balance:

$$\delta_i = f_{carb}\delta_{carb} + f_o\delta_{org} \quad (1)$$

where δ_i is the isotopic composition of all carbon entering the surface environment, and f_{carb} and f_o represent the fractions of carbon deposited as carbonate rock and organic matter, respectively. This equation can be rearranged with carbonate $\delta^{13}C$ as the subject:

$$\delta_{carb} = \delta_i + (f_o\Delta\delta^{13}C) \quad (2)$$

where $\Delta\delta^{13}C$ (or ε_{TOC}) is the carbon isotopic discrimination between deposited carbonate rock and organic matter [7].

Interpretations of global trends in $\delta^{13}C_{carb}$ generally involve the assumption that both δ_i and $\Delta\delta^{13}C$ are invariant, which allows $\delta^{13}C_{carb}$ to be translated solely in terms of C_{org} burial. This assumption has arisen because the $\delta^{13}C$ compositions of the major sources of oceanic carbon, weathering, volcanism and metamorphism, will approximate bulk crust and upper mantle $\delta^{13}C$, that is -5 to $-7‰$ [8–10], over geological time-scales, while $\Delta\delta^{13}C$ has been empirically determined at about $25 \pm 5‰$ [10]. As a result, periods of very high $\delta^{13}C$ ($> +10‰$), such as during the mid-late Neoproterozoic (Cryogenian) [11–16], are interpreted to reflect prolonged episodes of high organic carbon burial rates [17,18]. Such episodes of disproportionately high burial of reduced carbon are believed to have caused stepwise increases in surface oxygen availability during Earth history [17,18]. However, on time-scales shorter than about 100 Ma, changes in both δ_i and $\Delta\delta^{13}C$ can be envisaged [10,19–21], which may invalidate interpretations of $\delta^{13}C_{carb}$ in terms of changes in C_{org} burial only.

We propose that global changes in δ_i and $\Delta\delta^{13}C$ occurred during the Neoproterozoic, and that these would have had a significant effect on seawater $\delta^{13}C$. First, we consider that carbonate weathering-related increases in δ_i (based on discussions in [21]) may help to explain the almost ubiquitous connection between positive $\delta^{13}C_{carb}$ excursions and cooling/regression during the late Neoproterozoic (and early Palaeozoic). Then we use $\delta^{13}C$ data from carbonate/C_{org} pairs to assess the possible influence of global changes in $\Delta\delta^{13}C$ on $\delta^{13}C_{carb}$ during the Neoproterozoic. Lastly, we use other geochemical and sedimentological arguments to constrain the likely effects of basin restriction and locally enhanced vertical gradients in $\delta^{13}C$ due to redox stratification on the $\delta^{13}C_{carb}$ record. This enables us to ascertain how representative $\delta^{13}C_{carb}$ data are of the spatially averaged global surface ocean. All these parameters need to be constrained before measured values of $\delta^{13}C_{carb}$ can be referred to changes in global carbonate versus organic carbon burial rates, especially for $\delta^{13}C_{carb}$ excursions of limited duration (< 100 Ma). Unravelling the relative importance of these parameters will help towards a better understanding of the interplay between the global carbon cycle, surface oxygenation and the evolution of the biosphere.

2. Tsagaan Gol section

2.1. Geological setting

The Neoproterozoic part of the Tsagaan Gol Section (Khasagt–Khayrkhan range, Altai Province, western Mongolia) is a single, non-composite section, with clear evidence for glaciation [22]. At Tsagaan Gol, two discrete glacial episodes are recorded as diamictites separated by 200 m of siliciclastic rocks, which are interpreted to include at least one shoaling-upward sequence [22]. At the top of the upper diamictite, and overlying slumps of glaciogenic material, finely bedded limestones of the Tsagaan Oloom Formation progress upward into shelly fossil-bearing limestones [14] of the lowermost Cambrian or uppermost Precambrian 600 m above in sequence 6 (Fig. 1). This Neoproterozoic part of the Tsagaan Oloom Formation is divided into at least three shoaling-upward sequences bounded by disconformities showing karstic collapse and brecciation. There are no characteristic cap carbonates [4,23] overlying the diamictites in Tsagaan Gol and similar facies have not been reported from elsewhere in the region.

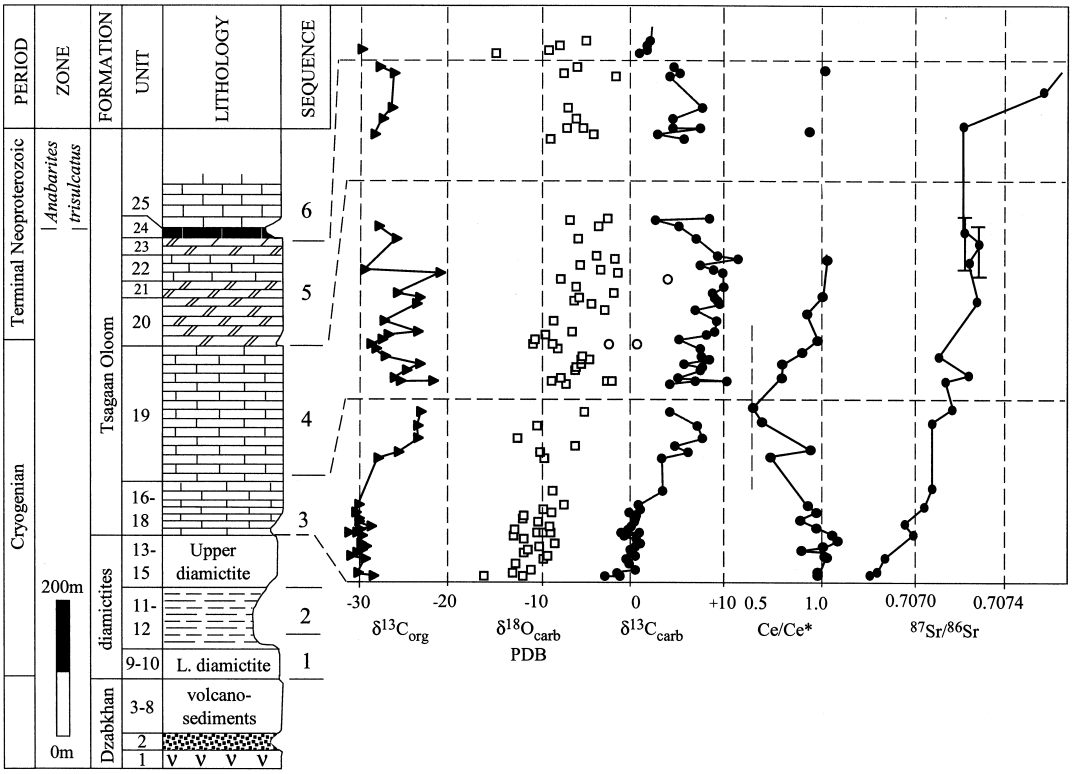

Fig. 1. Tsagaan Gol Section (Precambrian part), western Mongolia with geochemical data. The relative thicknesses of sequences 3 and 4 have been expanded to allow better comparison of geochemical data.

2.2. Age and global correlation

Global correlation of barren, Neoproterozoic sections can be attempted using a combination of Sr and C-isotope stratigraphy [24–26]. The first post-glacial sequence at Tsagaan Gol reveals a significant rise in $^{87}Sr/^{86}Sr$ of 450×10^{-6} from 0.70675 to 0.70722, followed by a plateau of $^{87}Sr/^{86}Sr$ values around 0.7072 (±0.0001) through the second post-glacial sequence 4 [14,27]. A similar rise in $^{87}Sr/^{86}Sr$ from 0.7066 to 0.7071 from the Twitya to the Keele Formations of the MacKenzie Mountains, NW Canada [3] suggests stratigraphic correlation of the two Tsagaan Gol diamictites with the mid-Neoproterozoic Rapitan (= Sturtian) glacial episode, dated at ca. 750–725 Ma [26]. In NW Canada, the later glacial episode, the Ice Brook, is accompanied by $^{87}Sr/^{86}Sr$ ratios of 0.7071 both above and below as well as unusually high $\delta^{13}C$ below the glacial level [3,12]. These isotope characteristics are matched in Mongolia either side of the sequence 4/5 boundary (Fig. 1), which we consider corresponds to this Ice Brook level (= Marinoan) glaciation, ca. 600 Ma. A 'Sturtian' or mid-Neoproterozoic affinity for the Tsagaan Gol diamictites is consistent with reported radiometric ages from the unconformably underlying Dzabkhan volcanic suite of between 770 and 725 Ma [14].

2.3. Carbonate petrography

The Neoproterozoic part of the Tsagaan Gol Section is represented by limestones with rarer dolostones. Zones of limited exposure occur along the Tsagaan Gol valley (Table 1), which generally represent finer-bedded intervals that are less carbonate-rich. The very base of the Tsagaan Oloom Formation consists of several meters of pale gray, poorly or non-laminated dusty microspar, which

Table 1
Petrographic and geochemical data for Tsagaan Gol section carbonate rocks

Sample	Unit	Microfabric	Height (m)	% sol.	$\delta^{13}C$	$\delta^{18}O_{PDB}$	$\delta^{13}C_{org}$	$\Delta\delta^{13}C$	TOC (%)	C/S	Ce/Ce*	$^{87}Sr/^{86}Sr$[a]
96TST1A	16	con. lam. msp.	0.1	95.2	−3.3	−16.6	−28.9	25.6	0.13	9.4	0.97	0.70675[a]
96TST1a	16	con. lam. msp.	0.1	98.1	−1.7	−12.4	−28.9	27.2	0.08	12.5		
96TST2	16	con. lam. msp.	1.5	98.0	−2.0	−13.5	−30.6	28.7	0.08	11.4	0.97	0.70680[a]
96TST3	16	con. lam. msp.	3.0	96.5	0.1	−11.4			0.12	12.5		
96TST5	16	con. lam. msp.	6.0	97.8	−0.6	−13.1			0.09	9.7		
96TST6	16	con. lam. msp.	7.5	97.1	−0.9	−10.1	−29.8	28.9	0.10	14.8		0.70684[a]
96TST7	16	con. lam. msp.	9.0	97.9	0.1	−9.7	−31.4	31.5	0.08	12.2	1.04	
96TST8	16	msp.	10.5	96.6	−0.3	−12.3	−30.8	30.5	0.05	7.1	1.02	
96TST9	16	con. lam. msp.	12.0	97.6	−0.4	−11.8	−30.2	29.7	0.17	15.1	0.84	
96TST10	16	con. lam. msp.	13.5	97.4	0.0	−10.5	−29.7	29.7	0.18	13.5	1.02	
96TST11	16	con. lam. msp.	15.0	98.3	0.6	−8.9	−30.3	30.9	0.11	8.1	1.11	
96TST12	16	con. lam. msp.	16.5	97.8	0.2	−12.2			0.13	15.7		
96TST13	16	con. lam. msp.	18.0	97.6	−1.2	−13.4	−30.1	28.9	0.39	13.4	1.07	0.70699[a]
96TST14′	16	con. lam. msp.	19.5	97.3	−1.5	−10.8	−31.6	30.1				
96TST14″	16	con. lam. msp.	19.5	97.3	−1.2	−10.1	−30.8	29.6	0.11	8.2		
96TST14	16	con. lam. msp.	19.5	98.4	0.6	−9.3			0.11	14.4		
96TST15	16	discon. lam. msp. and det.	21.0	93.6	−0.7	−13.2	−30.4	29.7	0.16	19.2		
96TST16	16	con. lam. msp.	22.5	98.2	−0.3	−9.5	−29.1	28.8	0.10	14.0	0.99	0.70694[a]
96TST17	16	discon. lam. msp.	24.0	98.1	0.0	−10.7	−30.5	30.5	0.32	24.3	0.84	
96TST18	16	discon. lam. msp.	25.5	97.7	0.1	−12.4	−30.5	30.7	0.29	18.8	0.93	
96TST19	16	msp. and wispy pellicles	27.0	98.0	0.2	−12.3						
96TST20	16	pel. micrite and mat rip-ups	28.5	98.8	−0.5	−9.2	−30.9	30.4	0.14	22.8		
96TST21	16	pel. micrite and mat rip-ups	30.0	97.5	0.7	−10.1			0.22	21.8		0.70705[a]
96TST22	16	Fe-rich cc. sp. and det.	31.5	98.0	0.5	−7.9	−30.5	30.9	0.28	18.0	0.89	
Poor exposure												
96TST24	17	dark micrite and pellicles	38	90.1	3.2	−9.1			0.50	42.5		0.70709[a]
96TST26	17	v. dark pell. msp. and mic.	52	86.9	3.0	−10.0	−28.4	31.4	0.54	28.2	0.64	
Main exposure												
96TST27	18	clotted micrite and det.	55	78.4	5.9	−10.4	−26.1	32.1	0.30	8.1	0.92	
96TST28	18	clotted micrite (thromb.)	58	93.4	4.5	−6.6			0.25	16.2		
96TST29	18	clotted micrite (thromb.)	61	93.0	7.6	−12.9	−23.9	31.5	0.44	62.5		
96TST31	18	dolospar	67	97.6	7.0	−10.8	−23.9	31.0	0.44	14.8	0.58	0.70709
96TST32	18	pell. micrite; disrupted	70	98.5	3.8	−7.1						
96TST33	18	patchy msp.; disrupted	73	99.0	3.9	−5.6	−23.6	27.5	0.27	48.5	0.52	0.70720[a]

Table 1 *(continued)*

Sample	Unit	Microfabric	Height (m)	% sol.	$\delta^{13}C$	$\delta^{18}O_{PDB}$	$\delta^{13}C_{org}$	$\Delta\delta^{13}C$	TOC (%)	C/S	Ce/Ce*	$^{87}Sr/^{86}Sr$[a]
Karst horizon												
96TST35	19	msp. and cc. veins	77	99.7	3.9	−7.6			0.03	26.6	0.71	0.70716
96TST36a	19	cc. sp.	87	99.4	6.8	−9.2	−25.9	32.7				
96TST36b	19	cc. sp.	87	99.3	10.3	−2.5	−22.2	32.5	0.07	25.2		
96TST37	19	cc. msp.	97	99.9	4.9	−8.2	−26.5	31.5	0.06	29.0		0.70729
96TST39	19	cc. msp.	117	98.0	7.3	−6.6	−25.2	32.5	0.18	17.2	0.73	
96TST40	19	discon. lam. msp.	127	99.5	7.6	−6.5			0.18	55.0		
96TST41	19	discon. lam. msp.	137	99.4	5.5	−5.9	−23.7	29.2	0.13	48.0		
96TST42	19	discon. lam. msp.	147	99.5	8.3	−5.0					0.84	0.70713
96TST42′	19	discon. lam. msp.	147	99.5	7.8	−5.9						
96TST43	19	micrite and patchy cc. sp.	157	99.8	7.5	−5.8	−27.6	35.1	0.12	51.0		
No exposure												
96TST46	19	micrite and patchy cc. sp.	182	91.7	7.4	−8.5	−28.6	35.9	0.09		0.96	
96TST47	19	micrite and patchy cc. sp.	194	97.5	−2.8	−9.1	−29.2	26.4	0.07	27.9		
96TST48	19	grapestone oosparite	206	99.8	5.0	−11.0	−27.9	32.8	0.10	65.1		
96TST49	19	con. lam. msp., dis.	218	99.8	8.0	−9.9	−27.2	35.2	0.12	36.9		
96TST50	19	con. lam. msp., dis.	230	99.7	8.9	−6.9	−23.9	32.8	0.17	45.0		
Poor exposure												
96TST52	19	con. lam. msp., dis.	260	99.6	9.2	−9.0	−27.7	36.9	0.12	24.6	0.89	
Main exposure												
96TST53	19	con. lam. msp.	290	99.7	6.8	−3.3			0.12	34.8		
96TST55	19	mic., patchy sp. and dol.	310	99.7	9.5	−4.8	−24.0	33.5	0.07	47.0	1.01	0.70734
96TST56	19	con. lam. msp., dis.	320	99.8	9.2	−6.7			0.10	29.6		
96TST57	19	con. lam. msp., dis.	330	99.3	9.0	−6.2	−23.7	32.7	0.11	21.5		
96TST58	19	msp.	340	99.7	8.7	−2.2	−26.2	34.9	0.08	70.5		
96TST60	19	msp.	360	99.8	10.0	−6.4			0.09	26.6		
96TST62	19	msp., sp.	380	99.5	3.7	−8.2			0.11	32.8		
96TST64	19	mic., msp.	400	99.9	9.8	−1.8	−21.5	31.3	0.02	30.6	1.03	
96TST65	19	mic., msp.	410	99.6	8.8	−3.8	−29.8	38.6	0.06	35.9		
96TST66	19	mic., msp.	420	98.8	7.4	−6.1			0.07	14.9		0.70729
96TST68	19	msp., sp. and dol.	440	99.8	11.6	−2.2			0.04	16.6		
96TST69	19	dolomsp.	450	97.0	9.2	−4.2						0.70735[a]
No exposure												
96TST70	19	dolosp.	500	93.8	6.9	−6.2	−26.3	33.2		10.6		
No exposure												
96TST71	19	dolosp.	550	91.7	2.4	−7.2						0.70725[a]
96TST72	19	coarse dolosp.	555	91.7	8.3	−3.0			0.88			

Table 1 *(continued)*

Sample	Unit	Microfabric	Height (m)	% sol.	$\delta^{13}C$	$\delta^{18}O_{PDB}$	$\delta^{13}C_{org}$	$\Delta\delta^{13}C$	TOC (%)	C/S	Ce/Ce*	$^{87}Sr/^{86}Sr$[a]
Karst horizon												
96TST73	20	mic. and msp.	556	99.6	4.9	−3.9	−28.2	33.1	0.06	33.4		
96TST74	20	msp	620	99.0	2.6	−4.5	−28.6	31.2			0.93	
96TST75	20	dark msp. and det.	624	95.0	7.3	−7.4						0.70725[a]
96TST85	20	dusty sp. and minor dol.	672	94.1	4.4	−6.3	−28.1	32.5	0.32	8.0		
No exposure												
96TST83	21	sp. and minor dol. crystals	617	87.2	5.5	−9.3			0.73	22.1		
96TST82	21	sp.	624	98.0	4.3	−5.7			0.34	28.7		
96TST81	21	dusty msp.	631	96.7	4.3	−6.5	−27.7	32.0	0.23	42.7		
96TST80	21	dusty sp.	638	88.7	7.6	−7.3	−26.7	34.3	0.22	9.4	1.01	
No exposure												
96TST77	22	dolmicrite and dsp.	660	98.9	4.0	−2.0			0.01	3.0		0.70769[a]
96TSTLT1	22	cc. sp.	662	98.1	5.0	−7.9	−26.5	31.6	0.16	47.7		
96TSBG3	23	*Boxonia grumulusa* dol.			4.1	−10.5						
	24											
96TSLTU(L)	25	cc.	700		0.6	−16.1						
96TSLTU(1)	25	cc.	714		1.4	−10.1						
96TSLTU4	25	cc.	718		1.5	−8.8						
96TSLTU5	25	cc.	722		1.8	−5.9						

con. = continuously; lam. = laminated; msp. = microspar; sp. = spar; dol. = dolomite; cc. = calcite; det. = significant detritus; discon. = discontinuously; pell. = pellicle-rich; pel. = peloidal; mic. = micritic; dis. = disrupted or slumped; thromb. = thrombolitic texture. $Ce/Ce^* = 3(Ce/Ce_{PAAS})/\{(2La/La_{PAAS})+(Nd/Nd_{PAAS})\}$; PAAS: Post-Archean Australian Shale [28]). $^{87}Sr/^{86}Sr$ data are discussed elsewhere [14,25,27].

[a] Refers to $^{87}Sr/^{86}Sr$ results from different samples but at an equivalent stratigraphic level [14,25,27].

directly overly several decimeters of greenish and reddish shale. Overlying this level, the limestone (unit 16) is laminated with common color-banded alternations of fine and coarse calcite spar, with crystals up to 1 mm in diameter. Laminations are continuous with spar growth being strictly confined to within the laminae. A gradual transition occurs through sequence 3 to discontinously laminated microsparite and micrite in unit 17, showing a peloidal microstructure and with darker, floating wispy pellicles. After a detritus-rich, ferrous calcite-bearing interval of friable and patchy exposure, the same pellicle-rich, microspar fabric continues as before, with some evidence for mechanical disruption of the pellicles (unit 18). In some instances the pellicles reveal crinkly textured internal layering, indicating a microbial origin. Clusters of coarser microsparite or sparite can be observed within the micrite, which are assigned to Catagraphia Maslov or more specifically *Vesicularites*. Some samples of unit 18 show the characteristic clotted texture of a thrombolite with intervening pores filled or lined with cement. At the top of the sequence, one bed of interlocking dolospar and calcitic oncolites sits below a surface of bauxitic karst. Sequence 3 has been interpreted as generally shoaling-upward through a suboxic zone represented by the ferrous calcite interval [27].

Sequence 4 initially follows the opposite trend from non-laminated micrite with occasional grapestones and oolites to fine-bedded laminated limestones, which show considerable syn-depositional microslumping and microfaulting.

3. Methods

Pure calcite powders were made from chips picked from crushed thin-section counterparts. The techniques used for calcite C, and O- isotope geochemistry have been described previously [14,25,27]. Organic carbon isotope ratios were measured after repeated treatment with concentrated hydrochloric acid at Lausanne Stable Isotope Laboratory using a Carlo Erba Elemental Analyzer coupled to a Delta S Finnigan Mat Mass Spectrometer, and are normalized to the standard NBS 21 ($\delta^{13}C = -28.1$‰ PDB). Rare earth element (REE) concentrations were measured on acetic acid, HCl, HNO_3 or α-hiba reagent (pH 4.5)-soluble fractions at the CGS, Strasbourg by inductively coupled plasma mass spectrometry. No significant difference in cerium anomaly or REE pattern was observed in five samples using these variously mild and harsh techniques, implying that all the REE are located in the easily soluble, most likely carbonate, fraction. H/C and C/S ratios, and total organic carbon (TOC) were analyzed on decarbonated limestone samples using a C–N–S–H elemental analyzer at the University of Ottawa.

4. Results

Our data reveal an increase in $\delta^{13}C_{carb}$ above the Tsagaan Gol diamictites from −3 to +11‰. $\delta^{13}C_{org}$ ranges equally in both post-glacial sequences but shows erratic scatter in sequence 4 (between −30 and −21‰) compared with a smooth climb in sequence 3 (from −32 to −23‰). $\delta^{18}O_{calcite}$ increases up-section, too, from an average of −13‰ PDB at the base to −5‰ through the upper part of sequence 4. TOC ranges between 0.02 and 0.9% in these samples, averaging 0.2%. S contents are generally low with C/S ratios ranging between 7 and 65, averaging 25. H/C ratios for 13 C-rich (>25% carbon by weight) decarbonated residues were measured at between 0.25 and 0.50. Ce depletion, expressed as a Ce anomaly, where $Ce/Ce^* = 3(Ce/Ce_{PAAS})/\{(2La/La_{PAAS})+(Nd/Nd_{PAAS})\}$; PAAS = Post-Archean Australian Shale [28]), becomes progressively more prominent through sequence 3 (Ce anomaly = 1.1–0.5) and then disappears towards the upper half of sequence 4 (Ce anomaly = 0.6–1.1).

5. Discussion of carbon isotope data

5.1. Diagenetic alteration

Strontium isotope and trace element considerations (low Mn/Sr, Fe/Sr, high [Sr]) indicate that the Tsagaan Gol limestones are geochemically well preserved at least in terms of their trace element compositions [14,27]. However, diagenetic alteration of the carbon isotopic system may be unrelated to these inorganic diagenetic indicators, so independent arguments for the faithful preservation of $\delta^{13}C$ values are necessary. First, changes in $\delta^{13}C_{org}$ through sequence 3 mirror those of $\delta^{13}C_{carb}$ remarkably well, which is consistent with the preservation of primary variations in both $\delta^{13}C_{carb}$ and $\delta^{13}C_{org}$ in sequence 3 [6]. Second, $\Delta\delta^{13}C$ is high, being greater than 28‰ throughout. This suggests that the effects of diagenetic alteration on both $\delta^{13}C_{carb}$ and $\delta^{13}C_{org}$ have been limited as alteration of either of these parameters would normally cause $\Delta\delta^{13}C$ to decrease because reequilibration with organic-bearing fluids tends to decrease $\delta^{13}C_{carb}$, while thermal maturation tends to increase $\delta^{13}C_{org}$ [10,11,29]. Third, H/C ratios >0.25, together with the low metamorphic grade of the Tsagaan Gol carbonates, indicate that thermal maturation has prob-

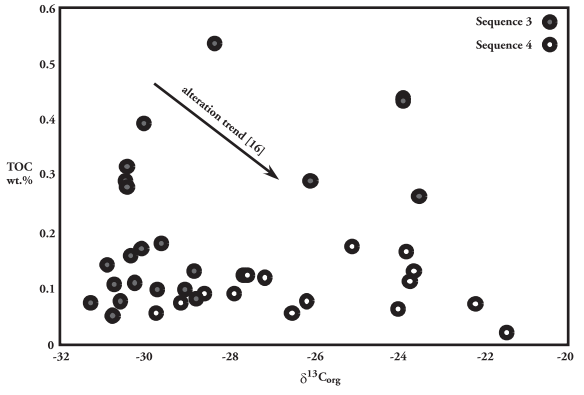

Fig. 2. Crossplot of TOC (kerogen content) versus $\delta^{13}C_{org}$.

ably caused only a minor increase in $\delta^{13}C_{org}$ after deposition of less than 3‰ [29]. Fourth, there is no correlation between TOC and $\delta^{13}C$ (Fig. 2) as commonly occurs in cases where there has been systematic loss of ^{12}C during alteration [16]. Together, these considerations imply that the $\delta^{13}C_{carb}$ excursions and high $\Delta\delta^{13}C$ from our study are primary phenomena. Below, we assess possible interpretations of high $\delta^{13}C$ in Cryogenian seawater.

5.2. High $\delta^{13}C$ due to high C_{org} burial rates?

High $\delta^{13}C_{carb}$ values up to 10–16‰ have been reported from many Neoproterozoic sections worldwide [11–16], the highest values being arguably restricted to the interval between the two major Neoproterozoic glacial intervals, i.e. ca. 720–600 Ma [7,18,24–26]. As discussed in Section 1, it is assumed by convention that δ_i and $\Delta\delta^{13}C$ (from Eq. 2) are fairly constant over geological time-scales, which allows us to make direct inferences about the proportion of carbon burial as organic matter relative to total carbon deposition (f_o). If we assume typical Phanerozoic values for $\delta_i \sim -5$‰ and $\Delta\delta^{13}C \sim 25$‰, we can use Eq. 2 to arrive at an estimate of f_o equal to 0.64, compared with f_o of about 0.25 during most of the Phanerozoic [7]. A more realistic value for mean $\Delta\delta^{13}C$ over geological time is now considered to be 28–32‰ [7], which leads to an estimate for f_o of between 0.50 and 0.57, which is still anomalously high, and implies unusually elevated organic carbon burial rates [11] that are as yet unsupported by the sedimentary record. At present, our knowledge of the deep ocean sedimentary realm is too poor to confirm or reject the hypothesis of high organic burial rates during much of the Neoproterozoic. However, the validity of some of the assumptions that led to this hypothesis are open to question.

5.3. High $\delta^{13}C$ due to high δ_i?

Although δ_i must correspond to bulk crustal $\delta^{13}C$ in order to attain the mass balance in Eq. 1, this need not be the case on time-scales of considerably shorter than 100 Ma [29]. Potentially the most variable source of ocean carbon is surface weathering, the isotopic composition of which depends strongly on the proportion of carbonate versus organic matter weathering. Therefore, changes in the source of ancient weathered carbon may affect δ_i.

Changes in δ_i have been invoked to explain high $\delta^{13}C_{carb}$ during the latest Ordovician (Hirnantian) and at three times during the Silurian (Llandoverian, Wenlockian and Ludlovian) [21]. Using the Hirnantian episode as an example, carbonate $\delta^{13}C$ reached +7‰, while $\Delta\delta^{13}C$ also attained high values of between 36 and 39.5‰ (in Nevada) [21] as in our Mongolian data. In that study it was considered that regression itself could have been a factor in causing high seawater $\delta^{13}C$, by exposing huge areas of low-lying platform carbonates to karstic weathering, and thus increasing δ_i. The possible magnitude of such a change remains unconstrained at present but the authors propose an increase in δ_i of 4‰.

Similar changes to δ_i can be envisaged for parts of the Neoproterozoic due to the repetition of glacially related eustatic regressions that would have uncovered the enormous expanses of older low-lying stromatolite-covered cratons, which are characteristic of the lower Neoproterozoic and upper Mesoproterozoic in Africa, South America, Canada, Australia and Siberia. A connection between trends to high $\delta^{13}C$ and regression, including karstic features in carbonate terrains, has been observed for the Neoproterozoic [16,27] and throughout the early Palaeozoic [21,30,31], which is consistent with changing δ_i due to increased carbonate weathering. Major regressions during times of increasing seawater $\delta^{13}C$ would also lead to the exposure of carbonates progressively more enriched in ^{13}C, thus causing a short-term runaway effect of increasing δ_i, and surface seawater $\delta^{13}C$.

5.4. High $\delta^{13}C$ due to high $\Delta\delta^{13}C$?

Seawater $\delta^{13}C$ may also be affected by changes in $\Delta\delta^{13}C$, and so this parameter should be constrained by analyzing carbonate/C_{org} pairs. At Tsagaan Gol, $\delta^{13}C_{carb}$ rises from −3 to +7.5‰ through the first post-glacial sequence, a rise

shadowed by a parallel $\delta^{13}C_{org}$ increase from −32 to −23‰ (Fig. 1). The difference between these two trends, $\Delta\delta^{13}C$, is roughly invariant at around 30‰ (±1.5‰), which is a typical value for all Neoproterozoic to Mesozoic rocks [7]. A recent carbon isotope study from a post-Sturtian section in Australia [16] reports identical $\delta^{13}C_{carb}$, $\delta^{13}C_{org}$ and $\Delta\delta^{13}C$ results from correlative post-glacial strata there.

Through sequence 4 in Mongolia, as in the pre-Marinoan of Australia and the pre-Ice Brook of NW Canada, $\delta^{13}C_{carb}$ continues to rise to 11‰. In contrast to the lower post-glacial sequence, $\delta^{13}C_{org}$ displays considerable fluctuation between −30 and −23‰ through this upper sequence. Values of $\Delta\delta^{13}C$ in the upper sequence, 32–39‰, are consistently as high or higher than the highest of the lower sequence. Such $\Delta\delta^{13}C$ values are too high to be the result of primary production even under extreme conditions of pCO_2, where photosynthetic fractionation, or ε_p, may reach 25‰ and overall isotopic discrimination 32‰ [7]. As discussed above, high $\Delta\delta^{13}C$ values are also unlikely to result from post-depositional alteration and thermal maturation. The only currently plausible explanation for such high $\Delta\delta^{13}C$ involves microbial reworking [32]. Most secondary processes tend to enrich organic matter in ^{13}C, thus decreasing $\Delta\delta^{13}C$, however, reworking by non-photosynthetic chemoautotrophic bacteria may cause further enrichment of ^{12}C in organic matter [7]. The most likely location of such microbial reworking is within the zone of organic matter respiration within the redox transition, which can be situated close to the sediment–water interface or within the water column. Therefore, such elevated values of $\Delta\delta^{13}C$ may reflect a local intensification of this redox boundary.

One unusual aspect of the Mongolian $\delta^{13}C_{org}$ data from sequence 4 is their inconsistency at any particular stratigraphic level (Fig. 1). This has also been noted elsewhere in sediments with high $\Delta\delta^{13}C$ [21,33] and may be explained by the range in $\delta^{13}C$ that would result from the mixing of different proportions of primary and secondary organic matter.

Although increases in $\Delta\delta^{13}C$ would certainly alter the $\delta^{13}C$ composition of the remaining carbon in the ocean reservoir, these changes need to be truly global to have any effect on seawater $\delta^{13}C$. In a recent compilation of stable isotope data covering the last 800 Ma, $\Delta\delta^{13}C$ of over 32‰ was systematically found beneath Neoproterozoic glacial sedimentary units [7], although few $\Delta\delta^{13}C$ values exceeded 35‰ during times of $\delta^{13}C_{carb} > 10‰$. Considering that measured $\delta^{13}C_{org}$ is likely to be slightly altered by maturation by up to 2‰ even in well preserved organic matter, it could be justifiably hypothesized that $\Delta\delta^{13}C$ was as high as 37‰ globally at this time, but no higher. Using Eq. 2 again, and assuming $\delta_i = -5‰$, f_o between 0.25 and 0.5, and $\Delta\delta^{13}C$ between 30 and 37‰, high $\Delta\delta^{13}C$ could cause an increase in seawater bicarbonate $\delta^{13}C$, and thus $\delta^{13}C_{carb}$ of between 1 and 3‰, which, although significant, is insufficient on its own to explain the Cryogenian $\delta^{13}C_{carb}$ excursions.

5.5. *High $\delta^{13}C$ due to unrepresentative sampling and basin restriction?*

A common assumption in carbon isotope stratigraphy is that the measured $\delta^{13}C_{carb}$ data from shallow-marine carbonate rocks of one area are representative of carbonate rocks worldwide. Knowledge of the whole ocean isotopic composition is not required for the isotope balance in Eqs. 1 and 2, but instead, only that of the spatially averaged surface ocean [34]. Nevertheless, we still need to test the global significance of any isotopic excursion before using it for isotope or mass balances. Firstly, although Neoproterozoic isotopic records from different regions of the world can be quite similar, implying correlation [24–26], it is still desirable to establish by independent means that apparently identical $\delta^{13}C_{carb}$ excursions are contemporaneous. This is particularly difficult in the absence of stratigraphically useful fossil assemblages, and avoiding use of the $\delta^{13}C$ data themselves for correlation, which would lead to circular reasoning. As a result, it cannot yet been demonstrated beyond doubt that Neoproterozoic $\delta^{13}C_{carb}$ peaks are globally contemporaneous features of the surface ocean. Despite this uncertainty, we note that all major $\delta^{13}C_{carb}$ excursions of the early Palaeozoic have been shown to

be globally contemporaneous where biostratigraphic correlation has been sufficiently precise for this purpose [14,21,31].

Secondly, even if the global significance of a $\delta^{13}C$ feature can be demonstrated, it may be that all related $\delta^{13}C$ data derive from basins with restricted access to global seawater, thus causing estimates of global surface ocean $\delta^{13}C$ to be exaggerated. In such cases, high $\delta^{13}C$ may result from locally, and not globally, high rates of organic burial. If the partly anoxic W. Mongolian (Dzabkhan) Basin were one of a number of such basins unconnected with the rest of the global ocean, high $\delta^{13}C$ due to locally enhanced carbon storage might not have to imply globally elevated rates of organic burial. However, the widespread nature of high $\delta^{13}C$ and the consistency of $\delta^{13}C$ maximum values during the non-glacial Neoproterozoic indicate that the governing factor over high $\delta^{13}C$ was global in scope and that the global surface ocean $\delta^{13}C$ was indeed anomalously high at this time. Future stratigraphic work will help to constrain further any possible effects of global $\delta^{13}C$ inhomogeneity.

5.6. High $\delta^{13}C$: the role of ocean redox stratification?

Establishing anoxic versus oxic conditions of deposition is especially difficult in the Neoproterozoic because the use of bioturbation indices as redox indicators is impossible due to the absence of burrowing metazoans. As an alternative approach, we studied the trace element distributions in the Tsagaan Oloom Formation limestones. Redox stratification causes enormous variability in iron, manganese and cerium concentrations due to their relative insolubility under oxidizing conditions. In a stratified basin, Ce, Mn and Fe concentrations are likely to be low in surface oxic waters, and higher at depth, with highest concentrations within the suboxic zone of redox-recycling [35]. Such characteristic depth-related distributions in ancient carbonate rocks would provide strong evidence for the existence of ocean stratification. Our earlier study [27] identified a trend towards Ce depletion (negative Ce anomalies), as well as Fe and Mn depletion, through sequence 3 above the upper glacial level at Tsagaan Gol, which might be taken as evidence for a trend towards oxygenation of the site of deposition during regression. The present study confirms this trend in an unrelated second set of samples and shows additionally that Ce depletion disappears progressively through sequence 4. C/S ratios (Table 1) mirror changes in Ce anomaly, and may also be related to changing redox conditions.

REE concentrations in limestones are liable to misinterpretation due to their rehomogenization during early diagenesis [36,37]. However, the existence of a strong Ce anomaly around the sequence 3/4 boundary is unambiguous because post-depositional alteration is unlikely to deplete cerium with respect to the other REE [36]. Therefore, cerium anomalies must indicate oxic conditions in local seawater around the sequence 3/4 boundary. The association of greater Ce depletion during basin shallowing [30,36] is not typical of a well mixed ocean, the reverse case being the normal situation today, and is only found in regions of water column anoxia [36]. Therefore, our cerium anomaly data are consistent with local redox stratification, and imply that samples yielding high $\delta^{13}C$ ($>+7‰$) around the sequence 3/4 boundary were deposited above any redox boundary within the water column. Conversely, samples from the base of sequence 3 and from higher up in sequence 4 were likely deposited in deeper waters close to or below any redox boundary.

The confirmed presence of ocean anoxia (redox stratification) in this basin implies a steep vertical seawater $\delta^{13}C$ gradient, which would affect our $\delta^{13}C$ record, and may be a partial explanation for the positive relationship between regression and $\delta^{13}C$ in our and others' data [16,33]. According to this scenario, a trend towards higher $\delta^{13}C$ may result from shallowing of the locus of deposition from below, to above, the redox boundary within the basin [27]. However, this scenario would only be valid if the measured limestones were all direct sea-floor precipitates, which is often not the case, having instead precipitated initially in surface waters as whitings. Where a sea-floor origin for the limestone can be entertained, redox-stratification coupled with sea-level change might be one possible cause of a $\delta^{13}C$ trend, in

which case some $\delta^{13}C$ excursions may neither be real nor global. In any case, although anoxia may enhance organic carbon preservation, thus increasing seawater $\delta^{13}C$, and may serve to increase vertical gradients in seawater $\delta^{13}C$, the mere presence of redox stratification will not increase surface seawater $\delta^{13}C$ and does not, therefore, explain the extremely high $\delta^{13}C$ values that are a characteristic feature of the Neoproterozoic. In the present case, few of the Tsagaan Oloom limestones from the base of the section to the top of sequence 4 show any evidence of having been precipitated at the sea-floor. Therefore, it is doubtful whether the trend to increasing $\delta^{13}C$ from -3 to $+11‰$ was caused by shallowing in a redox stratified setting, but instead must represent a temporal trend in seawater $\delta^{13}C$.

5.7. Some wider implications

The above discussions lead to the conclusion that there was a genuine increase in surface seawater $\delta^{13}C$ of around $10‰$ between the mid-Neoproterozoic and the late Neoproterozoic glacial episodes. In some regions, this shift was associated with regression and shallow ocean anoxia. An identical relationship between regression, shallow ocean anoxia and high $\delta^{13}C$ has been reported from the Ordovician–Silurian boundary [30]. The regression in this case corresponds to the latest Ordovician glacial maximum, before which there was a globally observed $\delta^{13}C$ excursion of up to $+7‰$, associated with $\Delta\delta^{13}C$ up to $39‰$ in Nevada [21]. This is sufficiently similar to the non-glacial Neoproterozoic case as to warrant speculation about shared mechanisms. In both these cases global cooling trends led to eustatic regression and shallowing of the locus of deposition in the presence of a strong redox barrier. The intensity of this redox barrier is recorded in the Ce anomaly and other trace element data, C/S ratios and elevated $\Delta\delta^{13}C$ values. Models to explain changing $\delta^{13}C$ during the Neoproterozoic and early Palaeozoic will need to keep such associations in mind before high $\delta^{13}C$ during this interval can be interpreted simply in terms of greater organic carbon burial and, therefore, global surface oxygenation.

6. Conclusions

Four factors may have led to anomalously high $\delta^{13}C$ in Cryogenian (late Neoproterozoic) limestones of western Mongolia and worldwide. First, a global increase in the fraction of carbon burial as organic matter may have increased seawater $\delta^{13}C$. However, such an increase is as yet unsupported by the sedimentary record. Second, exposure and weathering of widespread and low-lying early Neoproterozoic carbonate platforms during eustatic regression may have increased the $\delta^{13}C$ of weathering input to the ocean, which would also have contributed to elevated $\delta^{13}C$. This mechanism is especially relevant during the period of break-up of the supercontinent Rodinia that was dominated by stromatolite-covered cratons. The possible extent of changes in δ_i remains unconstrained at present. Third, an increase in global mean $\Delta\delta^{13}C$, related to an intensification of the redox barrier, may have been a minor contributing factor. Fourth, locally elevated $\delta^{13}C$ in restricted basins may have caused overestimation of global surface seawater $\delta^{13}C$ in some cases. In addition, redox stratification and related, high vertical chemical gradients in seawater may also have caused apparent positive $\delta^{13}C$ excursions during sea-level change, however, this cannot explain the overall elevation in $\delta^{13}C$ values during the Neoproterozoic. The commonly observed connection between cooling, regression, shallow ocean anoxia, and increasing $\delta^{13}C$ during the late Neoproterozoic and early Palaeozoic requires additional well constrained geochemical studies before it can be adequately explained. Unravelling these factors will help towards a better understanding of the role of the carbon cycle in past global environmental change, especially surface oxygenation and its effects on the evolution of the biosphere.

Acknowledgements

The authors gratefully acknowledge helpful and constructive reviews by David Des Marais, John Hayes, Lee Kump and Malcolm Walter. The instructive comments of Lee Kump, in particular,

led to a marked improvement in the quality of the manuscript. Thanks also to Viorel Atudorei, Albuquerque, USA, for carrying out the organic carbon isotope analyses. *[EB]*

References

[1] I.W.D. Dalziel, Neoproterozoic–Paleozoic geography and tectonics: review, hypothesis, environmental speculation, GSA Bull. 109 (1997) 16–42.
[2] B. Harland, Critical evidence for a great infra-Cambrian glaciation, Geol. Rundsch. 54 (1964) 45–61.
[3] A.J. Kaufman, A.H. Knoll, G.M. Narbonne, Isotopes, ice ages, and terminal Proterozoic earth history, Proc. Natl. Acad. Sci. USA 94 (1997) 6600–6605.
[4] P.F. Hoffman, A.J. Kaufman, G.P. Halverson, D.P. Schrag, A Neoproterozoic snowball, Earth Sci. 281 (1998) 1342–1346.
[5] A.H. Knoll, S.B. Carroll, Early animal evolution emerging views from comparative biology and geology, Science 284 (1999) 2129–2137.
[6] A.H. Knoll, J.M. Hayes, A.J. Kaufman, K. Swett, I.B. Lambert, Secular variations in carbon isotope ratios from upper Proterozoic successions of Svalbard and East Greenland, Nature 321 (1986) 832–838.
[7] J.M. Hayes, H. Strauss, A.J. Kaufman, The abundance of ^{13}C in marine organic matter and isotopic fractionation in the global biogeochemical cycle of carbon during the past 800 Ma, Chem. Geol. 161 (1999) 103–125.
[8] D.J. Des Marais, J.G. Moore, Carbon and its isotopes in mid-oceanic basaltic glasses, Earth Planet. Sci. Lett. 69 (1984) 43–57.
[9] M. Javoy, F. Pineau, H. Delorme, Carbon and nitrogen isotopes in the mantle, Chem. Geol. 57 (1986) 41–62.
[10] W.T. Holser, M. Schidlowski, F.T. Mackenzie, J.B. Maynard, Geochemical cycles of carbon and sulfur, in: C.B. Gregor, R.M. Garrels, F.T. Mackenzie, J.B. Maynard (Eds.), Chemical Cycles in the Evolution of the Earth, Wiley, New York, 1988, pp. 105–173.
[11] A.J. Kaufman, A.H. Knoll, Neoproterozoic variation in the C-isotopic composition of seawater: stratigraphic and biogeochemical implications, Precambr. Res. 73 (1995) 27–49.
[12] G.M. Narbonne, A.J. Kaufman, A.H. Knoll, Integrated chemostratigraphy and biostratigraphy of the upper Windermere Supergroup, NW Canada: implications for Neoproterozoic correlations and the early evolution of animals, Geol. Soc. Am. Bull. 106 (1994) 1281–1292.
[13] S.S. Iyer, M. Babinski, H.R. Krouse, F. Chemale Jr., Highly ^{13}C-enriched carbonate and organic matter in the Neoproterozoic sediments of the Bambuí Group, Brazil, Precambr. Res. 73 (1995) 271–282.
[14] M.D. Brasier, G.A. Shields, V.N. Kuleshov, E.A. Zhegallo, Integrated chemo- and biostratigraphic calibration of early animal evolution: Neoproterozoic-early Cambrian of southwest Mongolia, Geol. Mag. 133 (1996) 445–485.
[15] M.D. Brasier, G.A. Shields, Neoproterozoic chemostratigraphy and correlation of the Port Askaig glaciation, Dalradian Supergroup of Scotland, J. Geol. Soc. London 517 (2000) 909–914.
[16] D.M. McKirdy, J.M. Burgess, N.M. Lemon, X. Yu, A.M. Cooper, V.A. Gostin, R.J.F. Jenkins, R.A. Both, A chemostratigraphic overview of the late Cryogenian interglacial sequence in the Adelaide fold-thrust belt, South Australia, Precambr. Res. 106 (2001) 149–186.
[17] J.A. Karhu, H.D. Holland, Carbon isotopes and the rise of atmospheric oxygen, Geology 24 (1996) 867–870.
[18] A.J. Kaufman, S.B. Jacobsen, A.H. Knoll, The Vendian record of Sr- and C-isotopic variations in seawater: implications for tectonics and paleoclimate, Earth Planet. Sci. Lett. 120 (1993) 409–430.
[19] J.M. Hayes, Global methanotropy at the Archean-Proterozoic transition, in: S. Bengtson (Ed.), Early Life on Earth, Columbia University Press, Princeton, Nobel Symposium 84, 1994, pp. 220–236.
[20] L.A. Derry, C. France-Lanord, Neogene growth of the sedimentary organic carbon reservoir, Paleoceanography 11 (1996) 267–275.
[21] L.R. Kump, M.A. Arthur, M.E. Patzkowsky, M.T. Gibbs, D.S. Pinkus, P.M. Sheehan, A weathering hypothesis for glaciation at high atmospheric pCO_2 during the Late Ordovician, Palaeogeogr. Palaeoclim. Palaeoecol. 152 (1999) 173–187.
[22] J.L. Lindsay, M.D. Brasier, G. Shields, V.V. Khomentovsky, Y.A. Bat-Ireedui, Glacial facies associations in a Neoproterozoic back-arc setting, Zavkhan Basin, SW Mongolia, Geol. Mag. 133 (1996) 391–402.
[23] M.J. Kennedy, B. Runnegar, A.R. Prave, K-H. Hoffmann, M.A. Arthur, Two or four Neoproterozoic glaciations, Geology 26 (1998) 1059–1063.
[24] S.B. Jacobsen, A.J. Kaufman, The Sr, C and O isotopic evolution of Neoproterozoic seawater, Chem. Geol. 16 (1) (1999) 37–57.
[25] G.A. Shields, Towards a new calibration scheme for the Terminal Proterozoic, Eclog. Geol. Helv. 92 (1999) 221–233.
[26] M.R. Walter, J.J. Veevers, C.R. Calver, P. Gorjan, A.C. Hill, Dating the 840–544 Ma Neoproterozoic interval by isotopes of strontium carbon, and sulfur in seawater, and some interpretative models, Precambr. Res. 100 (2000) 371–433.
[27] G.A. Shields, P. Stille, M.D. Brasier, N-V. Atudorei, Stratified oceans and oxygenation of the late Precambrian environment: a post-glacial geochemical record from the Neoproterozoic of W. Mongolia, Terra Nova 9 (1997) 218–222.
[28] S.M. McLennan, Rare earth elements in sedimentary rocks; influence of provenance and sedimentary processes, in: B.R. Lipin, G.A. McKay (Eds.), Geochemistry and Mineralogy of Rare Earth Elements, Reviews in Mineralogy 21, 1989, pp. 169–200.

[29] D.J. Des Marais, Isotopic evolution of the biogeochemical carbon cycle during the Proterozoic eon, Org. Geochem. 27 (1997) 185–193.
[30] K. Wang, B.D.E. Chatterton, M.Jr. Attrep, C.J. Orth, Late Ordovician mass extinction in the Selwyn Basin, northwestern Canada: geochemical, sedimentological, and paleontological evidence, Can. J. Earth Sci. 30 (1993) 1870–1880.
[31] M.R. Saltzmann, R.L. Ripperdan, M.D. Brasier, K.C. Lohmann, R.A. Robison, W.T. Chang, S. Peng, E.K. Ergaliev, B. Runnegar, A global carbon isotope excursion (SPICE) during the Late Cambrian: relation to trilobite extinctions, organic-matter burial and sea level, Palaeogeogr. Palaeoclim. Palaeoecol. 162 (2000) 211–223.
[32] J. Samuelsson, H. Strauss, Stable carbon and oxygen isotope geochemistry of the upper Visingsö Group (early Neoproterozoic), southern Sweden, Geol. Mag. 136 (1999) 63–73.
[33] S.D. Pell, D.M. McKirdy, J. Jansyn, R.J.F. Jenkins, Ediacaran carbon isotope stratigraphy of South Australia: an initial study, Trans. R. Soc. S. Aust. 117 (1993) 153–161.
[34] L.R. Kump, Interpreting carbon-isotope excursions Strangelove oceans, Geology 19 (1991) 299–302.
[35] C.R. German, B.P. Holliday, H. Elderfield, Redox cycling of rare earth elements in the suboxic zone of the Black Sea, Geochim. Cosmochim. Acta 55 (1991) 3553–3558.
[36] G.A. Shields, P. Stille, Diagenetic constraints on the use of the cerium anomaly as a palaeoenvironmental indicator, Chem. Geol. 175 (2001) 29–48.
[37] C.R. German, H. Elderfield, Application of the Ce anomaly as a paleoredox indicator the ground rules, Paleoceanography 5 (1990) 823–833.